

Order–Disorder Transition in Poly(oxyethylene)–Poly(oxybutylene) Diblock Copolymers

Shao-Min Mai,[†] J. Patrick A. Fairclough,[‡] Ian W. Hamley,[§] Mark W. Matsen,^{||} Richard C. Denny,^{⊥,∇} Bai-Xia Liao,[#] Colin Booth,[†] and Anthony J. Ryan^{*,‡,⊥}

Department of Chemistry, University of Manchester, Manchester M13 9PL, U.K., Manchester Materials Science Centre, UMIST, Grosvenor Street, Manchester M1 7HS, U.K., School of Chemistry and Centre for Self Organising Molecular Systems, University of Leeds, Leeds LS2 9TJ, U.K., Chemical Engineering and Materials Science, University of Minnesota, Minneapolis, Minnesota 55455, CCLRC Daresbury Laboratory, Warrington, WA4 4AD, U.K., Biophysics Section, Blackett Laboratory, Imperial College, London SW7 2BZ, U.K., and Department of Materials Science, Changsha Institute of Technology, Changsha, Hunan 410003, People's Republic of China

Received January 24, 1996; Revised Manuscript Received May 2, 1996[Ⓞ]

ABSTRACT: A series of poly(oxyethylene)–poly(oxybutylene) diblock copolymers have been prepared by anionic polymerization. The polymers were characterized by GPC and NMR and were found to have a narrow molar mass distribution. The structures of the melts were determined by SAXS, and peak shapes were found to be Lorentzian for disordered and Gaussian for ordered block copolymers. The structures of the melts agreed with the prediction of the self-consistent field theory (SCFT) phase diagram. The order–disorder transition was determined across a range of molecular weights, and these data were used to estimate the temperature dependence of χ , using a mean-field approximation, as $\chi = 48.5/(TK) - 0.0534$. The copolymers were found to be well segregated close to the ODT and had sharp interfaces with chains that were strongly stretched. The domain spacing was found to scale as $d \sim N^{0.69}$, in agreement with the SCFT prediction.

Introduction

Block copolymers are of fundamental scientific and commercial interest. They comprise two or more chemically different chains joined together (conventionally at their ends) by covalent bonds. Most commonly, the component chains are incompatible. If so, their material (bulk) properties are dominated by the tendency for the blocks to spontaneously separate into microphases when the temperature is lowered. This type of microphase separation occurs as a result of a reduction in enthalpy as the blocks demix, but at the cost of a loss of entropy as the blocks are arranged in ordered structures.¹ We report the synthesis of a series of diblock copolymers of ethylene oxide and 1,2-butylene oxide and their characterization in the bulk molten state. The copolymers are denoted E_mB_n , where E represents an oxyethylene unit [OCH_2CH_2] and B an oxybutylene unit [$\text{OCH}_2\text{CH}(\text{CH}_2\text{CH}_3)$]. Consideration has already been given^{2,3} to the structures formed from copolymers of this type in the micellar and gel states of their aqueous solutions. In the bulk state, the oxyethylene block is crystallizable and the oxybutylene block, which is atactic in microstructure, is noncrystallizable. The solid (semicrystalline) state of a limited range of E_mB_n copolymers has been previously reported.⁴ The melting points of the copolymers lie in the range 40–60 °C, and both the solid (semicrystalline) and liquid (noncrystalline) microphases of the copolymers are conveniently accessible to experiment. The emphasis in this paper is on the location of the order–disorder transition in the liquid state and the

determination of the temperature coefficient of the Flory–Huggins parameter χ using the mean-field approximation.

Theoretical and experimental aspects of microphase separation have been reviewed,^{1,5,21} and relevant references can be found therein. Starting from the pioneering studies of Helfand and Wasserman⁶ and Leibler,⁷ major contributions have come from self-consistent mean-field theories. Considering an AB block copolymer comprising $N = N_A + N_B$ chain units, each occupying the same volume (v) and having the same statistical length (b), theory predicts equilibrium phase behavior dependent only on the product χN and the composition defined by the mole fraction of (say) A chain units, $x_A = N_A/N$. For this special case, parameter b is uniquely determined by the radius of gyration of the copolymer,

$$R_g^2 = Nb^2/6 \quad (1)$$

and parameter χ by the noncombinatorial Gibbs energy of mixing

$$\Delta_{\text{mix}} G_{\text{nc}} = kT\chi N_A x_B = kT(\chi N) x_A x_B \quad (2)$$

For the copolymers of interest here, the unlike segments mix endothermically, and the temperature dependence of χ will be given approximately by

$$\chi = \alpha + \beta/T \quad (3)$$

where α and β are constants dependent on composition. Microphase separation is favored by lowering the temperature.

The main features of microphase separation in such a block copolymer system are clear. At low values of χN , the block copolymer comprises a single disordered phase in which the chains have unperturbed dimensions.^{1,7} Connectivity leads to a characteristic correlation length scaling as the radius of gyration, i.e., as $N^{1/2}$.

* To whom correspondence should be addressed.

[†] University of Manchester.

[‡] UMIST.

[§] University of Leeds.

^{||} University of Minnesota.

[⊥] CCLRC Daresbury Laboratory.

[∇] Imperial College.

[#] Changsha Institute of Technology.

[Ⓞ] Abstract published in *Advance ACS Abstracts*, August 1, 1996.

Microphase separation is predicted at $\chi N \approx 10$ (the weak segregation limit (WSL)). As the WSL is approached, theory⁸⁻¹³ predicts fluctuations in the disordered phase, with a characteristic dimension scaling as $N^{4/5}$. Immediately beyond the WSL, limited demixing of A and B occurs to form a microphase-separated phase with a characteristic dimension variously predicted⁹⁻¹³ to scale approximately as $N^{0.8}$ to $N^{0.95}$. In the strong segregation limit (SSL, $\chi N \gg 10$), AB contacts are limited to a narrow interfacial region, the microphases are essentially pure A and pure B, and the characteristic length is predicted⁴⁵ to scale as $N^{2/3}$.

In the SSL, any decrease in Gibbs energy resulting from minimization of interfacial area must be balanced against the resulting increase in Gibbs energy from the more extended chain conformation. Hence, at equilibrium in the SSL, the major phase-separated structures of BCC spheres, hexagonally packed cylinders and lamellae depend only on composition.¹ In the WSL, theory⁷ accounts for the same structures. The complex hexagonally perforated lamellar and cubic *Ia3d* mesophases (phases intermediate between the predicted structures) recently observed in weakly segregated diblocks¹⁴⁻²⁰ are not generally found to be the lowest energy structures by theory. The most recent theoretical work of Matsen and co-workers^{21,44} predicts the cubic *Ia3d* to be stable and hints at the conditions for stability of the perforated lamellar phases.

The assumption of equal volume and equal statistical length are overly restrictive in the application of theory to many block copolymers, including the E_mB_n copolymers of present interest. The problem has been discussed in a number of recent papers.^{4,22-24} In the Flory-Huggins treatment of mixtures of two polymers, eq 2 is recast in terms of volume fraction (ϕ) and number of segments (r_v). The two types of segments (E and B) each have the same reference volume, v_0 . For systems comprising E and B units, it is convenient to use the volume occupied by an E unit (v_E) as reference, whence

$$r_v = r_{vE} + r_{vB} = N_E + N_B(v_B/v_E) \quad (4)$$

where v_B is the volume occupied by a B unit. Room temperature values of the densities of liquid poly(oxyethylene) and poly(oxybutylene)⁴ lead to a value of $v_B/v_E \approx 1.89$. With values of χ based on the same reference volume, the equation for the noncombinatorial part of the free energy of mixing per chain, analogous to eq 2, is

$$\Delta_{\text{mix}} G_{\text{nc}} = kT(\chi r_v)\phi_E\phi_B \quad (5)$$

where ϕ_E and ϕ_B are volume fractions. This formulation requires a phase diagram plotted as χr_v versus, say, ϕ_E . If the two types of segment defined by volume have equal statistical lengths and if parameter χ is independent of concentration, then this phase diagram will be symmetrical in ϕ_E . Asymmetry in the phase diagram is caused by difference in statistical lengths, which enters through the radius of gyration. The unperturbed square radius of gyration is referenced to r_s segments of identical statistical length (b_0), in the present case put equal to that of an E unit: i.e.

$$R_g^2 = r_s b_E^2/6 \quad (6)$$

where

$$r_s = r_{sE} + r_{sB} = N_E + N_B(b_B^2/b_E^2) \quad (7)$$

With the chain length expressed in segments defined by volume,

$$R_g^2 = [r_{vE} + r_{vB}(v_E b_B^2/v_B b_E^2)]b_E^2 = [r_{vE} + \epsilon r_{vB}](b_E^2/6) \quad (8)$$

where parameter $\epsilon = (v_E b_B^2/v_B b_E^2)$ is equivalent to that described by Vavasour and Whitmore²³ and similar to that described by Almdal *et al.*^{19,24} Reported^{25,26} values of the unperturbed dimensions of poly(oxyethylene) and poly(oxybutylene) lead to $b_B^2/b_E^2 \approx 1.22$, whence $\epsilon \approx 0.65$. This is close to the value used by Vavasour and Whitmore ($\epsilon = 0.6$)²³ to illustrate the changes in the phase diagram to be expected from limited copolymer asymmetry, e.g., that typical of polystyrene-polydiene block copolymers. Following that work, it would be predicted that the microphase separation (disorder-order) boundary in the present system would be little changed from the hypothetical symmetrical case, but that the order-order boundaries would be affected, being significantly shifted toward higher volume fractions of oxyethylene (E). The order-disorder boundary used to systematically estimate χ from the ODT data is calculated in the mean-field approximation.⁷ We have calculated the phase boundaries using the incompressible Gaussian chain model and the self-consistent field theory (SCFT) of Helfand.⁴³ By using the numerical procedure introduced by Matsen and Schick,⁴⁴ we have calculated the mean-field phase diagram for $\epsilon = 0.6$ without invoking any of the traditional approximations, e.g., the narrow-interface and unit-cell approximations of Helfand and Wasserman⁶ or the Landau expansion and single-harmonic approximations of Leibler.⁷ Our phase diagram improves upon the Vavasour and Whitmore one²³ (also calculated for $\epsilon = 0.6$), which used approximations for the Wigner-Seitz unit cells of the HEX and BCC phases.

There is still some controversy over the choice of experiments used to locate the ODT. Rheological and scattering techniques^{28,29} are often used and some workers have also used the form birefringence as a diagnostic.³⁰ Measurements of rheological response and birefringence do not directly access thermodynamic parameters, but the changes observed do serve to locate the ODT provided that the data are correctly analyzed. Scattering from oriented samples in a temperature-dependent SAXS or SANS experiment may also be used to locate the ODT, the loss of orientation at the ODT resulting in a marked change in scattering pattern. According to the mean-field theory, there should be no discontinuous change in the X-ray scattering pattern from an unorientated sample at the ODT.⁷ However, so far as we are aware, there has been no report of scattering patterns from ordered or disordered block copolymers where the Leibler form⁷ of the scattering function could be fitted to the data without using the absolute intensity as an adjustable parameter. In fact, despite many early studies in which the intensity at the peak maximum, $I(q^*)$, has been observed to change continuously through the transition,^{1,32} there is now substantial agreement that there is a step change in $I(q^*)$ at the ODT and that the differential of the inverse peak position (q^*) with respect to inverse temperature ($\delta(1/q^*)/\delta(1/T)$) is constant, as was first pointed out by Bates and co-workers.³³ Hashimoto and co-workers have made many studies of ordering in block copolymers

Table 1. Molecular Characteristics of the Block Copolymers

copolymer	$M_n/g \text{ mol}^{-1}$	x_E	w_E	ϕ_E^a	r_v^b
series A					
E ₁₆ B ₂₂	2300	0.42	0.31	0.28	58
E ₃₇ B ₁₈	2900	0.67	0.56	0.52	71
E ₃₄ B ₁₂	2400	0.75	0.64	0.61	58
E ₅₀ B ₉	2800	0.85	0.77	0.74	67
series B					
E ₄₃ B ₂₃	3400	0.65	0.53	0.50	86
E ₅₆ B ₂₇	4400	0.67	0.56	0.52	107
E ₆₀ B ₂₉	4700	0.67	0.56	0.52	115
E ₇₄ B ₃₇	5900	0.67	0.55	0.51	144
E ₉₆ B ₄₇	7600	0.67	0.56	0.52	185
E ₁₁₄ B ₅₆	9000	0.67	0.55	0.52	220
E ₁₅₇ B ₇₆	12400	0.67	0.56	0.52	300
series C					
E ₁₁₅ B ₁₀₂	12400	0.53	0.41	0.38	308
E ₂₀₉ B ₄₅	12400	0.82	0.74	0.71	294

^a Calculated assuming densities of 1.12 and 0.97 g cm⁻³ for E and B, respectively. ^b E_mB_n : $r_v = m + (72/44)(1.12/0.97)n = m + 1.89n$.

using SAXS,³¹ and a recent publication³² reviews in detail the changes in peak intensity, $I(q^*)$, peak position, q^* , and peak width, σ , associated with the ODT.

In this work, we show, unequivocally, that the ODT in our copolymers can be located by SAXS *via* sharp transitions which are related to a change in peak shape, i.e., by transitions which take place within the temperature range defined by the sample–furnace temperature resolution. The ODT is also confirmed by low-frequency rheological measurements. Previous attempts to accurately determine the ODT by SAXS have been compromised by a combination of factors. The small-angle scattering cameras used previously have had relatively poor point-spread functions, due either to wide wavelength distributions (neutrons sources with $\Delta\lambda/\lambda$ typically 0.15) or to poor intrinsic collimation (laboratory X-ray sources with divergences of >100 mrad). Furthermore, the copolymers used have not had the necessary uniformity of chain length and composition allied to a low average molar mass to ensure rapid equilibration. We have minimized these problems by using a synchrotron SAXS camera with an improved resolution function together with specially synthesized low molar mass, narrow molar mass distribution, block copolyethers.

Experimental Section

(i) Synthesis and Characterization of Copolymers.

The copolymers were prepared by sequential anionic polymerization, first of ethylene oxide and then of 1,2-butylene oxide. All reagents were distilled and dried before use, and vacuum line and ampule techniques were used in order to minimize initiation by moisture at any stage. Initiator solution was prepared by reacting freshly cut potassium with 2-(2-methoxyethoxy)ethanol, the ratio [OH]/[OK] being adjusted to ensure a controlled rate of polymerization in the temperature range 45–65 °C. The method for copolymers with low number-average molar mass ($M_n < 5000 \text{ g mol}^{-1}$) has been described in detail previously.^{34,35} When preparing copolymers with higher molar mass ($M_n > 5000 \text{ g mol}^{-1}$), the reaction mixture became very viscous in the later stages, and higher temperatures (80–100 °C) were needed to ensure high conversion. The preparation of one such copolymer, E₉₆B₄₇, is described below. The prepared samples comprise three series, as indicated in Table 1: (A) $M_n \approx 2500 \text{ g mol}^{-1}$, ϕ_E from 0.28 to 0.74; (B) M_n from 2900 to 12 400 g mol⁻¹, $\phi_E \approx 0.5$; (C) $M_n \approx 12 400 \text{ g mol}^{-1}$, ϕ_E from 0.38 to 0.71, where ϕ_E is the volume fraction of E which the copolymer would have in its liquid state

at 25 °C. All samples were characterized by gel permeation chromatography (GPC) and nuclear magnetic resonance spectroscopy (NMR).

Two GPC systems were used. Samples of poly(oxyethylene) with short E chains (<E₈₀) and all block copolymers were examined using System I, which comprised three 30 cm PL-gel columns, one of porosity 500 Å and two mixed bed. The eluent was THF at 20 °C and a flow rate of 1 cm³ min⁻¹. Samples of poly(oxyethylene) with long E chains (>E₈₀) were examined using System II, which consisted of a similar column set, but with *N,N*-dimethylacetamide (DMA) at 65 °C and a flow rate of 1 cm³ min⁻¹ as eluent. In both systems, samples (concentration 2 g dm⁻³) were injected through a 100 mm³ loop, and emerging samples were detected by differential refractometry. Both systems were calibrated with a series of poly(oxyethylene) samples of known molar mass, and derived molar masses were based on poly(oxyethylene). Analysis of the GPC curve gave the molar mass at the peak (M_{pk}), while the width of the peak, corrected for instrumental spreading, gave an estimate of the ratio of mass-average to number-average molar mass (M_w/M_n). The GPC curves of certain block copolymers showed a small shoulder at low elution volume. This signal, generally corresponding to less than 1% of the whole, was attributed to a small fraction of triblock copolymer originating from difunctional poly(oxyethylene) initiated by adventitious moisture in the first stage of copolymerization. An exception was copolymer E₆₀B₂₉, the GPC curve of which showed a larger signal (*ca.* 5%) at low elution volume.

¹³C NMR spectroscopy was used to determine average composition (i.e., mole fraction or weight fraction E) and number-average molar mass. Polymer samples were dissolved in CDCl₃ (0.1 g cm⁻³) and spectra were obtained by means of a Varian Unity 500 spectrometer operated at 125.5 MHz. Spectral assignments were taken from previous work.³⁶ Integrals of resonances associated with end groups and chain groups were used to obtain the chain length of the poly(oxyethylene) prepared in the first stage of copolymerization, while those of chain groups (OCH₂CH₂ or OCH₂CH) and side groups (CH₂CH₃) were used to obtain the copolymer composition. A combination of these two quantities gave the overall molecular formulas of the copolymers.

¹³C NMR spectroscopy was also used to check the purity of the samples. For the precursor copolymers, the intensities of resonances from hydroxy-end-group carbons were compared with those from initiator carbons. Generally the two intensities were identical within experimental error (*ca.* 2 mol %). The spectrum of sample E₆₀B₂₉ indicated a 7 mol % excess intensity from hydroxy-end-group carbons, consistent with significant initiation by moisture. This difunctional polymer was converted to triblock copolymer in the second stage of copolymerization, as detected by GPC (see above). The purity of the block copolymers was checked by comparing the intensities of resonances from end-group carbons with those from carbons associated with EB block junctions. In most samples an excess (3–4 mol %) of hydroxy end groups over EB junctions was found. This was attributed to initiation of poly(oxybutylene) by moisture introduced with the second charge of monomer. The level of homopolymer impurity, which corresponded to *ca.* 2 wt %, was considered insignificant in view of the intended use of the samples in the bulk state. The copolymer compositions listed in Table 1 reflect the overall composition. The estimated uncertainty in block length is $\pm 5\%$.

(ii) **Details of the Synthesis of Copolymer E₉₆B₄₇.** The polymerization of ethylene oxide (39.7 g) was initiated by 2-(2-methoxyethoxy)ethanol partly in the form of its potassium salt (ratio [OH]/[OK] ≈ 9.63 , $9.24 \times 10^{-3} \text{ mol}$ of glycol plus salt). Polymerization was started at a temperature of 45 °C, which was increased to 65 °C (in order to prevent crystallization) until completion after 10 days. A small sample (0.31 g) of the polymer gave $M_{pk} = 4000 \text{ g mol}^{-1}$ and $M_w/M_n < 1.1$ from GPC System II, and 96 E units including end groups from NMR, corresponding to $M_n = 4200 \text{ g mol}^{-1}$ compared with $M_n = 4400 \text{ g mol}^{-1}$ expected.

The bulk of the poly(oxyethylene) (40.6 g) was used to initiate the polymerization of butylene oxide (34.0 g). Polymerization was started at 65 °C for 5 days, continued at 80 °C for 3 days, and finally held at 100 °C for 2 days to complete the reaction. The resulting copolymer had $M_{pk} = 7200 \text{ g mol}^{-1}$ and $M_w/M_n \approx 1.03$ from GPC System I. The GPC curve also indicated a small fraction (<1 wt %) of high-molar-mass material in the sample, attributable to triblock copolymer $B_{47}E_{192}B_{47}$. Overall, NMR gave $M_n = 7600 \text{ g mol}^{-1}$ and 56 wt % E (67 mol % E) compared with $M_n = 8200 \text{ g mol}^{-1}$ and 54 wt % E expected. In accordance with these overall results, the copolymer was denoted $E_{96}B_{47}$.

(iii) Time-Resolved Small-Angle X-ray Scattering. Measurements were made on beamline 8.2 of the SRS at the CCLRC Daresbury Laboratory, Warrington, UK. Details of the storage ring, radiation and camera geometry and data collection electronics have been given elsewhere.³⁷ The camera was equipped with a multiwire quadrant detector (SAXS) located 3.5 m from the sample position. A vacuum chamber placed between the sample and detectors reduced air scattering and absorption. Both the exit window of the beamline and the entrance window of the vacuum chamber were made from 15 μm mica, and the exit window of the vacuum chamber was made from 50 μm Kapton film. The spatial resolution of the SAXS detector was 400 μm and it could handle up to $\sim 500\,000$ counts s^{-1} . A beam stop was mounted just before the exit window to prevent the direct beam from hitting the SAXS detector, which measured intensity in the radial direction (over an opening angle of 70° and an active length of 0.2 m) and was only suitable for isomorphous scatterers. The specimens for SAXS were placed in a TA Instruments DSC pan containing a 0.75 mm brass spacer ring and fitted with windows (ca. 7 mm diameter) made from 25 μm thick mica. The loaded pans were placed in the cell of a Linkam DSC of single-pan design. The cell comprised a silver furnace around a heat-flux plate with a 3 \times 0.5 mm slot, the sample being held in contact with the plate by a low-thermal-mass spring. A more complete description of the DSC and the sample pans can be found elsewhere.³⁸ The scattering pattern from an oriented specimen of wet collagen (rat-tail tendon) was used to calibrate the SAXS detector and provide the conversion from pixel number to q ($= (4\pi/\lambda) \sin \theta$, where λ is the wavelength of the radiation and 2θ is the scattering angle). Parallel-plate ionization detectors placed before and after the sample cell recorded the incident and transmitted intensity.

In the present experiments, the temperature program was as follows: heat from room temperature to $T_{ODT} + 30 \text{ K}$ at 10 K min^{-1} , hold at maximum temperature for 1 min, and cool at 10 K min^{-1} to 10 K. In some cases, temperature ramps of 1 and 20 K min^{-1} were also applied to check for heating rate effects. The beamline data acquisition system had a time-frame generator which was programmed to collect the SAXS data in 6 s frames separated by a wait time of 10 μs . The experimental data were corrected for background scattering (subtraction of the scattering from the camera, hot stage, and an empty cell), for sample thickness and transmission, and for any departure from positional linearity of the detector.

(iv) Rheological Measurements. Rheological experiments were conducted with a Rheometrics RMS-800 dynamic mechanical spectrometer operated in the parallel-plate geometry. Specimens were prepared by melt pressing films of 1 mm in the 25 mm parallel-plate fixture of the rheometer. The furnace was heated at 2 K min^{-1} between measurement temperatures and held for 1 min at temperature prior to testing at 1, 10, and 100 rad s^{-1} . The furnace was flushed with dry nitrogen throughout the experiments and the samples were checked for degradation by GPC after heating. Samples that needed to be held at $T > 150 \text{ °C}$ had antioxidant (Stavox) added at the 150 ppm level.

Results and Discussion

The present study forms part of our systematic study of structure–property relationships in block copolymer systems. We have chosen to study E_mB_n copolymers since they exhibit complex microphases in the melt and

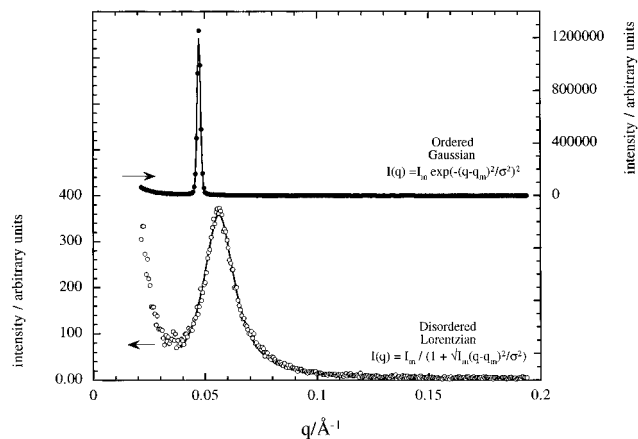


Figure 1. SAXS patterns for ordered and disordered melts of copolymer $E_{96}B_{47}$; the symbols are data points and the continuous lines are fits. The data for the disordered melt were fitted with a Lorentzian and those for the ordered melt with a Gaussian. The upturn at low q is of the same magnitude for the ordered and disordered samples and is due to parasitic scatter from the X-ray camera.

crystallization from the melt, allowing us to probe possible interrelationships between these two processes. However, the results and discussion that follow are restricted largely to the determination of the ODT and the temperature dependence of χ .

Copolymer $E_{96}B_{47}$. The general phase and scattering behavior of the copolymers of Series B ($\phi_E \approx 0.5$) is illustrated by the specific example of copolymer $E_{96}B_{47}$, which had an ODT intermediate between its melting point and the high-temperature limit of the experiments as determined by the thermal degradation of the samples.

SAXS patterns from copolymer $E_{96}B_{47}$ are shown in Figure 1. In order to illustrate clearly the difference between the scattering from ordered and disordered material, the patterns shown are those obtained from samples at temperatures 30 K apart on either side of the ODT. The peak obtained for the disordered material is best fitted by a Lorentzian function with $\sigma/q^* \approx 1/3$. This pattern is very similar to others in the literature.^{32,39} It could also be fitted with the full mean-field scattering profile given by

$$S^{-1}(q) = N^{-1}F(x, f) - 2\chi_{\text{eff}} \quad (9)$$

where χ_{eff} is an effective interaction parameter, $F(x, f)$ is a function relating to the correlation functions of a noninteracting (Gaussian) copolymer chain,⁷ and $x = (qR_g)^2$. In fact, as pointed out recently by Bates,³⁹ eq 9 is discriminating only if absolute intensities and the instrument resolution function are well known. Otherwise the values obtained for the fitting parameters (including χ_{eff}) are meaningless.^{32,39}

The peak for the ordered material (see Figure 1) is best fitted by a Gaussian function with $\sigma/q^* \approx 1/50$. This narrow peak is resolution limited, and is in fact the point-spread function of the instrument (combination of beam size and detector).⁴⁰ Just below the ODT, the sample most likely had a sinusoidal density profile^{1,7,8,32,39} with only a few Fourier modes overlapped around the mode with wave number q^* giving a very narrow peak. Most other workers have observed another Lorentzian for their ordered copolymers, probably due to wavelength dispersity,^{32,39} and possibly with a contribution to spreading from copolymer polydispersity.

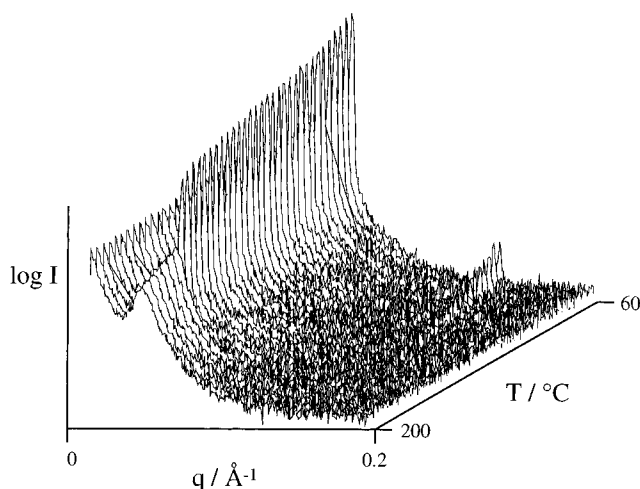


Figure 2. Three-dimensional relief diagram of time-resolved SAXS data obtained with a time resolution of 6 s during cooling copolymer of E₉₆B₄₇ from the disordered to the ordered phase. The full heating and cooling cycle was 10 → 200 → 10 °C at a ramp rate of 10 K min⁻¹. The plot shows log $I(q, t)$ versus scattering vector, q , versus temperature, T .

The transition from disorder to order (DOT) is illustrated in Figure 2 by a three-dimensional relief diagram of time-resolved SAXS data obtained with a time resolution of 6 s while cooling copolymer E₉₆B₄₇ from 200 (disordered) to 60 °C (ordered). The full heating and cooling cycle was 10 → 200 → 10 °C at a ramp rate of 10 K min⁻¹. The plot shows log $I(q, t)$ versus scattering vector, q , versus temperature, T . The change in line shape from Gaussian to Lorentzian on heating (and vice versa on cooling) occurred over a 3 K interval, and the intermediate patterns could be fitted by a weighted average of the two functions in a manner similar to that described by Sakamoto.³² There was significant hysteresis on heating and cooling, the difference in temperature being 8 K for E₉₆B₄₇ at a temperature ramp rate of 10 K min⁻¹. This behavior will be commented on below.

Considering the behavior of copolymer E₉₆B₄₇ on cooling below the DOT (see Figure 2), initially the ordered material had only one resolution-limited reflection in its SAXS pattern, but a third-order reflection (assuming lamellar microphase separation) appeared when the copolymer was cooled 20 K below the DOT. The second-order reflection was systematically absent, as expected for a symmetrical copolymer ($\phi_E = 0.5$) and lamellar microphase separation. This behavior is consistent with the sinusoidal composition fluctuation in the WSL becoming sharper with decreasing temperature, and eventually approaching a square wave,^{1,6,18,39} so giving rise to higher order reflections.

The SAXS data were fitted using the CCP13 (Collaborative Computational Project 13 for Fibre and Polymer Diffraction) program FIT.⁴¹ This applies a modified form of the Levenberg–Marquardt algorithm for nonlinear least-squares fitting to the problem of fitting time-resolved data. A Pearson VII function was used to define the peak shape, formulated as

$$I(q) = \frac{I(q^*)}{\left[1 + 4\left(\frac{q - q^*}{\sigma}\right)^2 (2^{1/\Psi} - 1)\right]^\Psi} \quad (10)$$

where $I(q^*)$ is the intensity at the peak maximum, q^* is the peak position, σ is the full width at half-

maximum, and Ψ is a shape parameter. $\Psi = 1$ corresponds to a Lorentzian, and as Ψ becomes large ($\Psi > 10$), the peak shape becomes approximately Gaussian. The Pearson VII parameters were obtained through the ODT by stepping through the data, the program automatically using the refined parameters from the fitting of the previous pattern as a starting model for the current pattern, and re-refining all four parameters of the Pearson VII function along with a polynomial background. As described below, the time (temperature) courses of the fitting parameters were subsequently used to determine the ODT.

In the region around the ODT the integrated intensity over the whole detector (also known as the relative invariant³⁸) was insensitive to the change in peak shape. The scattering in the sharp intense peak from the ordered material matched that in the broad peak from the disordered material.

As is usual in studies of this kind,^{9,18,24,28,32,33,39} the reciprocal peak position, $1/(q^* \text{Å}^{-1})$, and the reciprocal peak-maximum intensity, $1/I(q^*)$, were plotted as functions of reciprocal temperature, $1/(TK)$: see Figures 3A and 3B. The data shown were recorded during heating and cooling copolymer E₉₆B₄₇ in its liquid state between 25 and 190 °C. The melting temperature ($T_m \approx 60$ °C) and crystallization temperature ($T_c \approx 25$ °C) are marked. Values of $1/I(q^*)$ and $1/q^*$ obtained for the semicrystalline copolymer in the temperature interval T_m to T_c are not shown in Figures 3A and 3B, whereas data obtained for the undercooled liquid ($T < T_m$) of the ordered-liquid phase are shown.

The near reversibility of $1/q^*$ on heating and cooling is obvious from Figure 3A, particularly in the high-temperature range ($T > 130$ °C), and with small differences between values in the low-temperature range. The value of $1/q^*$ decreased with increasing temperature, which suggests that R_g decreases with temperature, as found for polyolefin^{9,18,39} and polystyrene–polydiene diblock copolymers.^{28,32} The expected³² temperature dependence of the peak position was found, i.e., straight-line behavior ($\delta(1/q^*)/\delta(1/T)$ constant). While there are data in the literature for the temperature dependence of R_g for PEO,⁴² as far as we are aware, there are no such data for the temperature dependence of R_g for PBO. It is not possible, therefore, to compare the temperature dependence of $1/q^*$ with that of R_g and thereby assess the degree of chain stretching.

As seen in Figure 3B, on heating copolymer E₉₆B₄₇ to temperatures above T_m , there were changes in $I(q^*)$ associated with annealing of the lamellar melt to a well-ordered phase. In the temperature range 60–140 °C, the scattering peaks observed for the heated copolymer were broad (see the inset to Figure 3C), i.e., consistent with scattering from small grains of ordered phase. We suppose that as temperature was increased from the melting point, residual grains of crystalline phase [broad peak, high $I(q^*)$, low $1/I(q^*)$] were replaced by small grains of ordered liquid phase [broad peak, low $I(q^*)$, high $1/I(q^*)$] followed by annealing to a material with long-range order over a large grain size [narrow peak, high $I(q^*)$, low $1/I(q^*)$]. Upon completion of the annealing process, the data for the heated sample coincided with those established for the cooled liquid ($T \approx 140$ °C: see Figure 3B). Over this whole low-temperature range ($T \approx 30$ –140 °C), the values of $I(q^*)$ found for the ordered liquid fell linearly with T as T was increased.

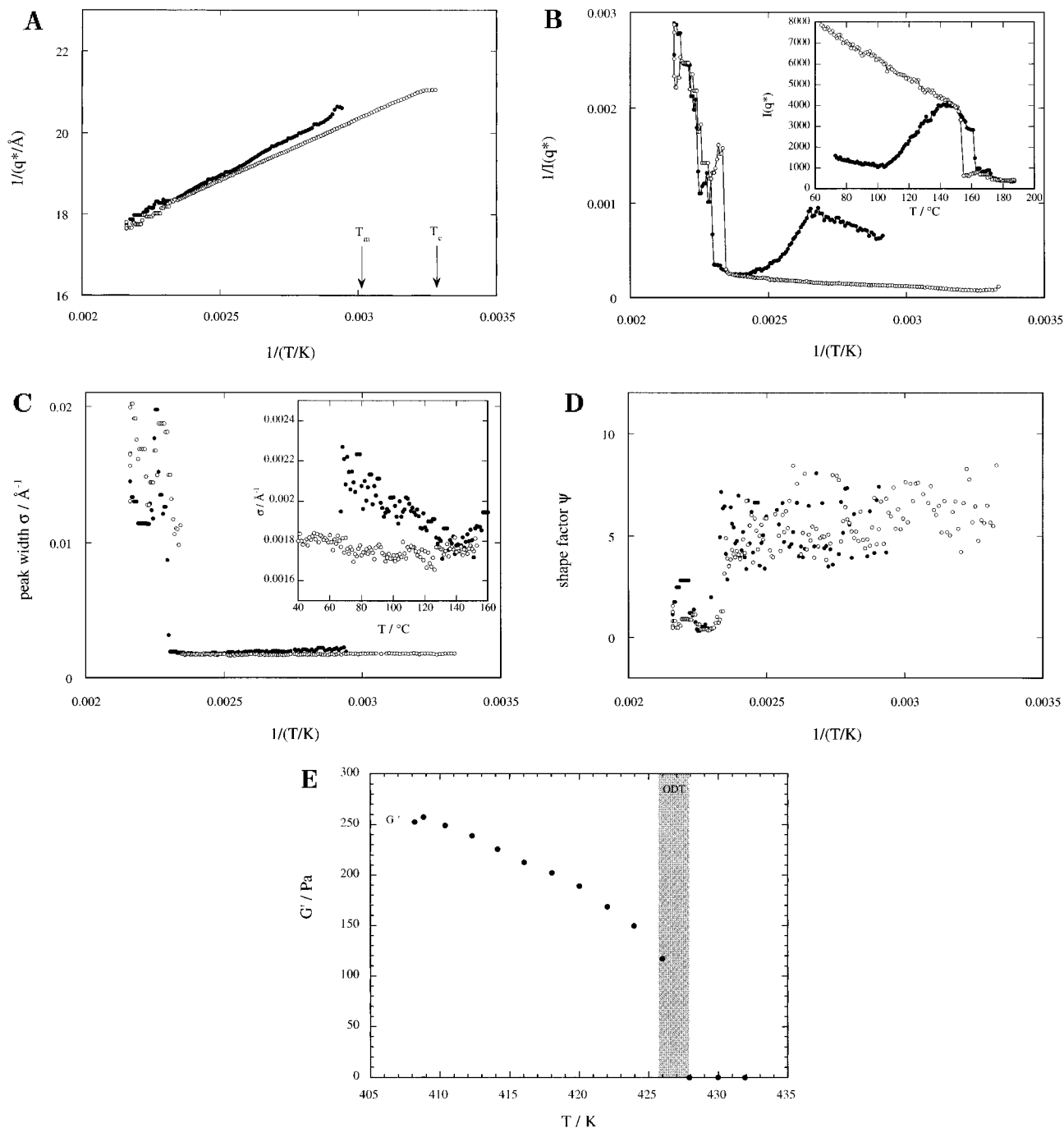


Figure 3. Various methods for determining the ODT; the closed symbols are for the heating ramp, and the open symbols are for cooling ramp. (A) reciprocal peak position, $1/(q^*/\text{Å}^{-1})$, as a function of reciprocal temperature, $1/(T/K)$. (B) reciprocal peak intensity, $1/I(q^*)$, as a function of reciprocal temperature, $1/(T/K)$. A plot of $I(q^*)$ versus T is included as an inset. (C) Peak width, σ , versus reciprocal temperature, $1/(T/K)$. The low-temperature data are plotted as a function of temperature, $T/^\circ\text{C}$. (D) The peak shape factor, Ψ (from fitting a Pearson VII peak to the data), versus reciprocal temperature, $1/(T/K)$. $\Psi = 1$ corresponds to a Lorentzian, and as Ψ becomes large ($\Psi > 10$), the peak shape becomes approximately Gaussian. (E) The in-phase shear modulus, G' , as a function of temperature. The ODT is marked as the shaded area.

The rapid changes in $I(q^*)$ on heating or cooling copolymer $E_{96}B_{47}$ at temperatures above 150°C (illustrated in Figure 3B) are associated with the order-disorder transition. There is some scatter in the data above the ODT if $1/I(q^*)$ is plotted, but nevertheless it is possible to characterize the effect as a step change in $I(q^*)$. The step is obvious if $I(q^*)$ is plotted against T , since this avoids compression of the abscissa in the region of interest and the noise in the data above the ODT is not accentuated. The inset to Figure 3B is $I(q^*)$ versus T .

The hysteresis (described above) is clearly seen in Figure 3B, the ODT (heating) occurring at a tempera-

ture some 8 K higher than the DOT (cooling). In this, the order-disorder transition resembles the crystal/melt transition, though the undercooling is larger for crystallization. As would be expected, the extent of hysteresis increased with increase in temperature ramp rate. Near-perfect reversibility of $I(q^*)$ was found if copolymer $E_{96}B_{47}$ was cycled between 10°C above T_m and 10°C below the ODT.

Discontinuities related to those in $I(q^*)$ were found at the ODT for the other parameters used in fitting the Pearson VII function to the diffraction pattern, i.e. the peak width (σ ; see Figure 3C) and the peak shape factor (ψ ; see Figure 3D). These plots show clearly the step

changes in these quantities at the ODT. The low values of σ and the high values of ψ at temperatures below the ODT ($\psi > 5$) are associated with the narrow, nearly-Gaussian-shaped scattering peak of the ordered phase. The corresponding high values of σ and low values of ψ above the ODT ($\psi \approx 1$) are associated with the wider Lorentzian-shaped peak. The transitions in both quantities are sharp, and there is significant hysteresis between the transition temperatures on heating and cooling the copolymer, much as noted above for $I(q^*)$ versus T . Hashimoto *et al.*^{28,32} discusses the peak width as being proportional to the reciprocal of the correlation length of the fluctuations, typically ≈ 500 Å for fluctuations of 140 Å, and if the same argument is applied to the ordered phase, then the ordered phase is polydomain with domains of ≈ 0.3 μm comprising lamellae of ≈ 140 Å.

The magnitudes of the steps in all three quantities [$1/I(q^*)$, σ , and ψ] were such that the transition temperatures could be readily defined to ± 1 °C. In comparing different methods and systems, Hashimoto *et al.*^{28,32} have used reduced parameters based upon the value of the quantity in the ordered and disordered phases. In a similar spirit, for the stepped quantities described above, we use $\Delta X/X_r$, where X denotes $1/I(q^*)$, σ , or ψ , ΔX denotes the absolute value of the step at the ODT, and X_r denotes the value of X in either the ordered or the disordered phase immediately below the ODT (depending on which is the larger in value). For copolymer E₉₆B₄₇, the values of $\Delta X/X_r$ found were as follows: inverse peak-maximum intensity $1/I(q^*) = 0.87$, peak width $\sigma = 0.8$, and peak shape $\psi = 0.83$. The value of $\Delta X/X_r$ for $1/I(q^*)$ can be compared with 0.79 obtained for a PS-PI copolymer²⁸ and 0.26 for a PEP-PEE copolymer.⁴⁰ Obviously, for an ordered phase with scattering pattern that is a delta function, the reduced discontinuity should be unity in the absence of line broadening.

In a separate experiment the ODT was determined by the step in the low-frequency (1 rad s⁻¹), in-phase shear modulus, G' , during a temperature ramp (heating rate 2 K min⁻¹ with a 1 min soak prior to each measurement). Rheological data for E₉₆B₄₇ are presented in Figure 3E. The ODT is determined with a precision of ± 1 K from the step function in G' which is associated with the loss of rigidity in the interfaces. The sharp nature of the ODT determined by rheology at an effectively zero heating rate compares with that determined by SAXS at a heating rate of 10 K min⁻¹.

Other E_nB_m Copolymers. Where the microphase transitions were accessible, the other copolymers (see Table 1) had similarly sharp ODTs and DOTs to those described for copolymer E₉₆B₄₇. The maximum in $1/I(q^*)$ associated with annealing of the melt to a well-ordered state was seen in all copolymers which had been crystallized. In all cases, the temperatures of the transitions were evident from step changes in the three quantities $I(q^*)$, σ , and ψ obtained from SAXS and the step change in G' from rheology. As described above, the temperatures of the ODT and the DOT were determined with a precision of ± 1 °C at a heating rate of 10 K min⁻¹ via the steps in the quantities $1/I(q)$, σ , and ψ , all three of which are associated with the change in the peak shape from the Lorentzian associated with the fluctuating melt to the Gaussian (resolution limited) associated with the sinusoidal density profile in the ordered melt. The results obtained are summarized in Table 2: i.e., the ODT temperatures, the temperature

Table 2. Scattering Data for the Block Copolymers

copolymer	r_v	ϕ_E	ODT/K		$\Delta T^a/\text{°C}$	$q^{*b}/\text{Å}^{-1}$	$d/\text{Å}$
			SAXS	rheo			
E ₄₃ B ₂₃	86	0.50	316 ^c	—	<i>c</i>	<i>d</i>	
E ₅₆ B ₂₇	107	0.52	326 ^c	322	<i>c</i>	<i>d</i>	
E ₆₀ B ₂₉	115	0.52	333	330	3	0.068	92
E ₇₄ B ₃₇	144	0.51	387	379	5	0.057	110
E ₉₆ B ₄₇	185	0.52	436	428	8	0.049	128
E ₁₁₄ B ₅₆	220	0.52	483	473	14	0.043	146
E ₁₁₅ B ₁₀₂	308	0.38	498	508	18	0.029	217 ^f
E ₁₅₇ B ₇₆	300	0.52	543	533	<i>e</i>	0.036	174
E ₂₀₉ B ₄₅	294	0.71	463	433	20	0.034	180

^a The difference between the ODT and DOT observed by SAXS at 10 °C min⁻¹. ^b q^* measured at 70 °C in the ordered phase. ^c DOT only, detectable for E₅₆B₂₇ and E₄₃B₂₃ on undercooling below T_m . ^d At 70 °C there was only the fluctuation scattering which did not allow accurate determination of q^* under the conditions employed in this work. ^e E₁₅₇B₇₆ held above the ODT degraded slightly. ^f Hexagonal phase.

differences between the ODT and the DOT, values of q^* in the ordered phase, and corresponding values of the periodicity $d = 2\pi/q^*$. Values of $\Delta X/X_r$ were found to decrease as molar mass was increased. As can be seen in the table, the extent of hysteresis increased with molar mass. The small discrepancies between the ODT determined by SAXS and rheological measurements are due mainly to differences in heating rate; however, some degradation of the polymer after long times at high temperatures cannot be ruled out.

Nature of the Transition. The large temperature differences between the ODT (heating) and the DOT (cooling) can be compared with the temperature-ramp effects associated with the liquid/crystal transition and the liquid-glass transition. The magnitudes of the hysteresis (see ΔT in Table 2), particularly for the high-molar-mass samples, are reminiscent of the undercoolings associated with the liquid/crystal transition, i.e., consistent with an activated process of nucleation and growth of the ordered phase from the disordered phase. This observation lends support to the designation of the temperature of the ODT (heating) as the correct indicator of the phase transition. Accordingly, we use the temperature of the ODT in further discussion.

Temperature Dependence of χ . In order to locate the copolymers on the mean-field phase diagram, the temperature dependence of χ is required, i.e., the coefficients in eq 3. To make some progress in this respect, values of χ at the ODTs of the symmetrical copolymers of Series B were calculated from the mean-field approximation of its critical value, $\chi_c = 10.5/r_v$, assuming χ to be independent of molecular weight. These values are plotted against the reciprocal of the transition temperature in Figure 4. The solid line is a least-squares fit to the data, i.e.

$$\chi = 48.5/T - 0.0534 \quad (T \text{ in K}) \quad (11)$$

This equation can be compared with $\chi = 34.1/T - 0.02$ found for PS-PI copolymers²⁸ and $\chi = 15.0/T - 0.0055$ found for PE-PEE copolymers.³⁹ We are well aware^{8,9,16-18,32,39} that the ODT is a transition from an ordered melt into a fluctuating melt and that using $\chi_c = 10.5/r_v$ underestimates the value of χ . The present experiments were designed primarily to locate the ODT, and give a reasonable estimate of the temperature derivative of χ but seriously underestimate its absolute value. In order to correct for fluctuation effects we would need to calculate the finite molar mass correction, $\tilde{N} (=Nb^3v^{-2})$, but this needs the temperature depen-

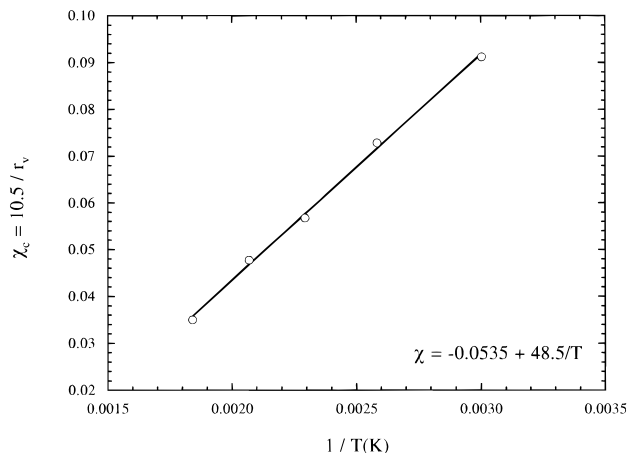


Figure 4. Value of the Flory-Huggins interaction parameter at the ODT (χ_c calculated from $10.5/r_v$) versus the reciprocal of the transition temperature for the symmetrical copolymers. The solid line is a least-squares fit to the data: $\chi = -0.0534 + 48.5/T$.

dence of the statistical segment length, b , and the molar volume, v , which are not currently available in the literature. While the lack of this data does not prevent us from estimating the required corrections, fluctuation theory⁸ does not strictly apply for $\bar{N} \leq 10^4$. We have already observed,⁴ in common with Bates and co-workers,³⁹ that the size of the fluctuation regime in these low-molar-mass copolymers is quite large (up to ≈ 50 °C). In a future communication, we will deal with fluctuation effects using a combination of X-ray and neutron scattering and rheology, which will allow a correct determination of χ . An estimate of the size of the \bar{N} correction is given later.

Phase Diagram. To complement the results obtained for the E_mB_n copolymer, we have calculated the phase boundaries using the incompressible Gaussian chain model and the self-consistent field theory (SCFT) of Helfand.⁴³ By using the numerical procedure introduced by Matsen and Schick,⁴⁴ we have calculated the mean-field phase diagram for $\epsilon = 0.6$ without invoking any of the traditional approximations, e.g., the narrow-interface and unit-cell approximations of Helfand and Wasserman⁶ or the Landau expansion and single-harmonic approximations of Liebler.⁷ Our phase diagram improves upon the Vavasour and Whitmore one²³ (also calculated for $\epsilon = 0.6$), which used approximations for the Wigner-Seitz unit cells of the HEX and BCC phases. In calculating the present diagram, we have limited our consideration to the classical structures, lamellae (LAM), hexagonally packed cylinders (HEX), and spheres on a body-centered-cubic lattice (BCC). Also stable theoretically²¹ are narrow regions of close-packed spheres along the ODT and regions between the LAM and HEX phases where the complex gyroid ($Ia3d$) phase is predicted; these structures will be accounted for in a subsequent publication.

The positions of the present E_nB_m diblock copolymers on the phase diagram have been calculated for a standard temperature of 55 °C using an apparent value of $\chi = 0.094$ given by eq 11. The open symbols in Figure 5 represent those copolymers with $T_m > T_{ODT}$ and the closed symbols those copolymers with $T_m < T_{ODT}$. The ODT is accessible on heating only for those copolymers represented by closed symbols which melt into an ordered phase.

Series A. The copolymers of Series A (low molar mass, various compositions) all melt directly into the

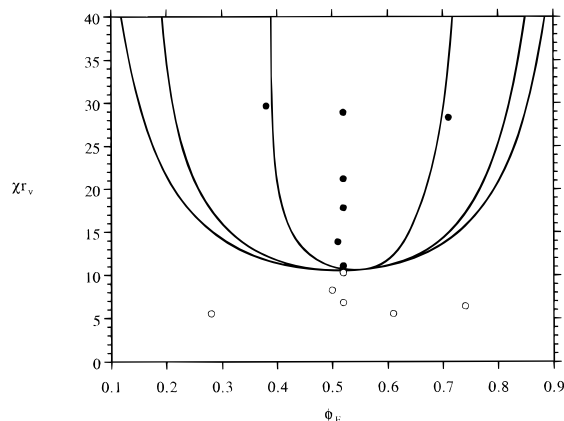


Figure 5. The positions of all the E_nB_m diblock copolymers, calculated for a melt temperature of 55 °C with $\chi = 0.094$, on a phase diagram calculated, using the numerical procedure introduced by Matsen and Schick,⁴⁴ from the incompressible Gaussian chain model and the self-consistent field theory (SCFT) of Helfand.⁴³ The open symbols represent those polymers with $T_m > T_{ODT}$ whereas the closed symbols represent those polymers with $T_m < T_{ODT}$.

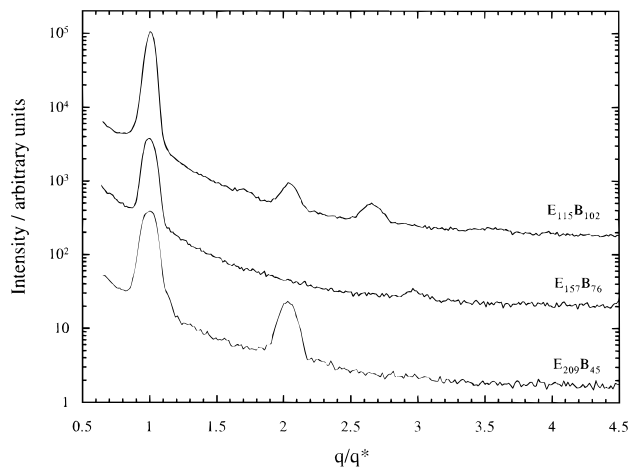


Figure 6. SAXS patterns for $E_{115}B_{102}$, $E_{157}B_{76}$, and $E_{209}B_{45}$. q^* is the value of q at the peak of the first-order reflection. Data for $E_{157}B_{76}$ and $E_{209}B_{45}$ have been shifted vertically for clarity.

disordered phase. These copolymers have very low scattering intensities in the disordered melt and only show fluctuation scattering, as was previously reported for other low-molar-mass E_nB_m copolymers.⁴

Series B. The symmetrical copolymers of Series B have lamellar morphologies in the ordered liquid phase, and the ODT is accessible on heating provided that $r_v > 115$. The data points for the two low-molar-mass copolymers of Series A ($E_{43}B_{23}$, $E_{56}B_{27}$) lie close to the phase boundary: see Figure 5. On heating them from the crystalline state at a rate of 10 K min^{-1} , they form melts with fairly intense Lorentzian scattering peaks arising from fluctuations. On cooling from the liquid state at 10 K min^{-1} , they can be supercooled below T_m into an ordered liquid phase prior to crystallization.

Series C. The nearly symmetrical copolymer $E_{157}B_{76}$ ($\phi_E = 0.52$), with reflections at q^* and $3q^*$ in the scattering pattern of Figure 6, is confirmed to be lamellar. Of the unsymmetrical copolymers of Series C, copolymers $E_{115}B_{102}$ ($\phi_E = 0.38$) and $E_{209}B_{45}$ ($\phi_E = 0.71$) both fall into the hexagonal regions of the theoretical phase diagram. However, SAXS patterns in Figure 6 show that while $E_{115}B_{102}$ produces peaks at q^* , $\sqrt{3}q^*$, $\sqrt{4}q^*$, $\sqrt{7}q^*$, and $\sqrt{11}q^*$ consistent with hexago-

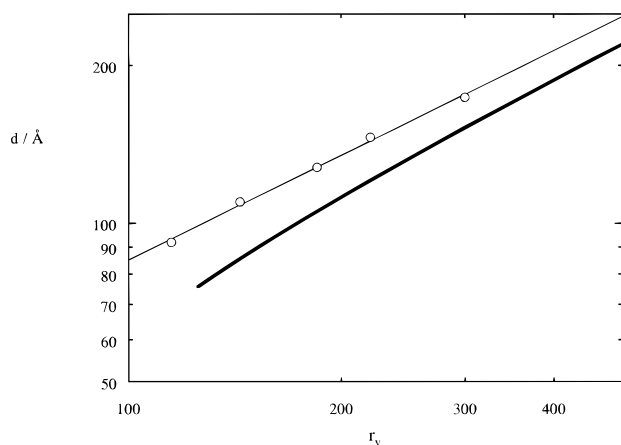


Figure 7. log–log plot of the fundamental length ($d = 2\pi/q^*$) of the polymer melt at 70 °C versus copolymer chain length in segments (r_v) for the lamellar copolymers. The measured spacings are the open data points and are fitted with a power law $d = 3.5r_v^{0.69 \pm 0.03}$. Theoretical spacings are given by the thick, solid line and are calculated from the SCFT.

nal symmetry, $E_{209}B_{45}$ produces peaks at q^* and $2q^*$, indicating lamellae. Although this might indicate that the actual value of ϵ is somewhat smaller than 0.6 and that the phase diagram is more skewed, this also could be a result of neglecting fluctuations in calculating χ . Because fluctuations shift the ODT to larger values of χr_v , χ is underestimated by assuming the mean-field value of the ODT. Shifting these data points up by only 5 units in χr_v (a modest fluctuation effect) brings them into the correct regions on the theoretical phase diagram.

Domain Size Scaling. Figure 7 shows a logarithmic plot of the lamellar spacing ($d = 2\pi/q^*$; see Table 2) versus the molecular size (r_v) for the compositionally symmetric ($\phi_E = 0.5$) diblocks at 70 °C. The experimental points are well fitted by

$$d = 3.5r_v^{0.69 \pm 0.03}$$

measured in angstroms. Also shown in Figure 7 is the theoretically calculated domain spacing. It is calculated using $\chi = 0.088$ and $R_g^2 = r_v(\phi_E + \epsilon\phi_B)b_E^2/6$ with $\phi_E = \phi_B = 0.5$, $\epsilon = 0.6$, and $b_E = 5.6 \text{ \AA}$.^{25,26} Theoretically, d increases most rapidly near the ODT. Away from the ODT at $r_v \sim 300$, the theoretical curve scales approximately as

$$d = 2.4r_v^{0.73}$$

We note that as the melts become increasingly segregated, the theoretical exponent is expected to approach a value of $2/3$.⁴⁵

The difference between experiment and theory can again be attributed to underestimating χ , as a result of not accounting for fluctuations. If χ is increased from 0.088 to something such as 0.2, then the theoretical and experimental results are virtually identical. This suggests that fluctuations effects are rather strong in this system and that the ODT has been moved to a χr_v value that is well into the intermediate-segregation regime. Specifically, it indicates that the ODT has been moved to about $\chi r_v \sim 0.2 \times 110 = 22$ as compared to ≈ 11 predicted by mean-field theory. We estimate that $\bar{N} = 3.7r_v$, which provides a value of about 400 near the ODT. With that value, the Fredrickson–Helfand theory⁸ predicts a shift of about 6 in the ODT due to fluctua-

tions. Considering that the Fredrickson–Helfand theory cannot be expected to work well for such a small \bar{N} , our estimated shift of 11 units in χr_v is not unreasonable.

Summary and Conclusions

We have prepared and characterized a series of diblock copolymers with well-defined compositions and narrow molar mass distributions. The structures of these copolymers in the melt were determined by SAXS: the low molar mass copolymers gave fluctuating melts irrespective of composition whereas higher molar mass copolymers gave ordered melts. The structure of the melts agreed (*with one exception*) with the prediction of the phase diagram calculated for the E_nB_m system, and the discrepancy between experiment and theory could be rationalized in terms of fluctuation effects being ignored and consequently χ being underestimated. Peak shapes were Lorentzian for disordered and Gaussian for ordered phases. The values of the ODT were identified by discontinuities in the intensity of the peak and the peak width and shape. On cooling from a high temperature, a melt with a single wide peak in its SAXS pattern passed through its DOT to form an ordered melt with one narrow reflection in its SAXS pattern, and on further cooling formed an ordered melt with higher order reflections in its SAXS pattern. These observations indicate a fluctuating melt at high temperature forming a melt with a sinusoidal composition modulation on cooling to the WSL, followed by a melt with a square-wave modulation on cooling to the SSL. The temperature dependence of χ was obtained from the dependence of the ODT on the copolymer length (r_v chain segments) and the mean-field approximation for microphase separation. The transition from WSL to SSL in these systems appears to occur at very low values of χr_v and this warrants further study.

Acknowledgment. Funding was provided for J.P.A.F. and R.C.D. under EPSRC Contract GR/K05982 and BBSRC Contract 28/X04460, respectively, and for S.M.M. by a University Scholarship and an ORS award. Beam time at Daresbury was provided by the EPSRC through the Materials SESS. The authors are grateful for the assistance of Ernie Komanschek in setting up the SAXS experiments and for discussions of SAXS data with Wim Bras. Practical help and advice came from Ga-Er Yu (synthesis), Keith Nixon (GPC), and Frank Heatley (NMR).

References and Notes

- (1) Bates, F. S.; Fredrickson, G. H. *Annu. Rev. Phys. Chem.* **1990**, *41*, 525.
- (2) Tanodekaew, S.; Deng, N.-J.; Smith, S.; Yang, Y.-W.; Attwood, D.; Booth, C. *J. Phys. Chem.* **1993**, *97*, 11847.
- (3) Yang, Y.-W.; Deng, N.-J.; Yu, G.-E.; Zhou, Z.-K.; Attwood, D.; Booth, C. *Langmuir* **1995**, *11*, 4703.
- (4) Yang, Y.-W.; Tanodekaew, S.; Mai, S.-M.; Booth, C.; Ryan, A. J.; Bras, W.; Viras, K. *Macromolecules* **1995**, *28*, 6029.
- (5) Brown, R. A.; Masters, A. J.; Price, C.; Yuan, X.-F. In *Comprehensive Polymer Science*; Booth, C., Price, C., Eds.; Pergamon: Oxford, 1989; Chapter 6.
- (6) Helfand, E.; Wasserman, Z. R. *Macromolecules* **1976**, *9*, 879; **1978**, *11*, 960; **1980**, *13*, 994.
- (7) Leibler, L. *Macromolecules* **1980**, *13*, 1602.
- (8) Fredrickson, G. H.; Helfand, E. *J. Chem. Phys.* **1987**, *87*, 697.
- (9) Almdal, K.; Rosedale, J. H.; Bates, F. S.; Wignall, G. D.; Fredrickson, G. H. *Phys. Rev. Lett.* **1990**, *65*, 1112.
- (10) Banaszak, M.; Whitmore, M. D. *Macromolecules* **1992**, *25*, 249.
- (11) Shull, K. R. *Macromolecules* **1992**, *25*, 2122.
- (12) Vavasour, J. D.; Whitmore, M. D. *Macromolecules* **1992**, *25*, 5477.

- (13) Muthukumar, M. *Macromolecules* **1993**, *26*, 5259.
- (14) Förster, S.; Khandpur, A. K.; Zhao, J.; Bates, F. S.; Hamley, I. W.; Ryan, A. J.; Bras, W. *Macromolecules* **1994**, *27*, 6922.
- (15) Hajduk, D. A.; Harper, P. E.; Gruner, S. M.; Honecker, C. C.; Kim, G.; Thomas, E. L. *Macromolecules* **1994**, *27*, 4063.
- (16) Schulz, M. F.; Bates, F. S.; Almdal, K.; Mortenson, K. *Phys. Rev. Lett.* **1994**, *73*, 86.
- (17) Hamley, I. W.; Koppi, K.; Rosedale, J. H.; Bates, F. S.; Almdal, K.; Mortenson, K. *Macromolecules* **1993**, *26*, 5959.
- (18) Bates, F. S.; Schulz, M. F.; Khandpur, A. K.; Förster, S.; Rosedale, J. H.; Almdal, K.; Mortenson, K. *J. Chem. Soc., Faraday Trans.* **1995**, *98*, 7.
- (19) Hamley, I. W.; Gehlsen, M. D.; Khandpur, A. K.; Koppi, K.; Rosedale, J. H.; Schulz, M. F.; Bates, F. S.; Almdal, K.; Mortenson, K. *J. Phys. II Fr.* **1994**, *4*, 2161.
- (20) Khandpur, A. K.; Förster, S.; Bates, F. S.; Hamley, I. W.; Ryan, A. J.; Bras, W.; Almdal, K.; Mortenson, K. *Macromolecules* **1995**, *28*, 8796.
- (21) Matsen, M. W.; Bates, F. S. *Macromolecules* **1996**, *29*, 1091.
- (22) Helfand, E.; Sapse, A. M. *J. Chem. Phys.* **1975**, *62*, 1327.
- (23) Vavasour, J. D.; Whitmore, M. D. *Macromolecules* **1993**, *26*, 7070.
- (24) Almdal, K.; Koppi, K. A.; Bates, F. S.; Mortensen, K. *Macromolecules* **1992**, *25*, 1743.
- (25) Beech, D. R.; Booth, C. *J. Polym. Sci., Part A-2* **1969**, *7*, 575.
- (26) Booth, C.; Orme, R. *Polymer* **1970**, *11*, 626.
- (27) Matsen, M. W. *Phys. Rev. Lett.* **1995**, *74*, 4225; *Macromolecules* **1995**, *28*, 5765.
- (28) Hashimoto, T.; Ogawa, T.; Han, C. D. *J. Phys. Soc. Jpn.* **1994**, *63*, 2206.
- (29) Koppi, K. A.; Tirrell, M.; Bates, F. S.; Almdal, K.; Mortensen, K. *J. Rheol.* **1994**, *38*, 999.
- (30) Balsara, N. P.; Garetz, B. A.; Dai, H. J. *Macromolecules* **1992**, *25*, 6072. Amundsen, K. R.; Helfand, E.; Patel, S. S.; Quan, Z.; Smith, S. D. *Macromolecules* **1992**, *25*, 1934.
- (31) Hashimoto, T.; Kowsaka, K.; Shibayama, M.; Kawai, H. *Macromolecules* **1986**, *19*, 754.
- (32) Sakamoto, N.; Hashimoto, T. *Macromolecules* **1995**, *28*, 6825.
- (33) Bates, F. S.; Rosedale, J. H.; Fredrickson, G. H. *J. Chem. Phys.* **1990**, *92*, 6255.
- (34) Luo, Y.-Z.; Nicholas, C. V.; Attwood, D.; Collett, J. H.; Price, C.; Booth, C. *Colloid Polym. Sci.* **1992**, *270*, 1094.
- (35) Bedells, A. D.; Arafeh, R. M.; Yang, Z.; Attwood, D.; Heatley, F.; Padgett, J. C.; Price, C.; Booth, C. *J. Chem. Soc., Faraday Trans.* **1993**, *89*, 1234.
- (36) Heatley, F.; Yu, G.-E.; Sun, W. B.; Pywell, E. J.; Mobbs, R. H.; Booth, C. *Eur. Polym. J.* **1990**, *26*, 583.
- (37) Ryan, A. J.; Macosko, C. W.; Bras, W. *Macromolecules* **1992**, *25*, 6277.
- (38) Bras, W.; Derbyshire, G. E.; Clarke, S.; Devine, A.; Komanschek, B. U.; Cooke, J.; Ryan, A. J. *J. Appl. Crystallogr.* **1994**, *28*, 26.
- (39) Rosedale, J. H.; Bates, F. S.; Almdal, K.; Mortenson, K.; Wignall, G. D. *Macromolecules* **1995**, *28*, 1429.
- (40) Hall, C.; Lewis, R.; Daresbury, private communication.
- (41) The programs used in data analysis are available from the Fibre and Polymer Diffraction Collaborative Computing Project CCP13 via the World Wide Web at the location <http://www.dl.ac.uk/CCP/CCP13/main.html>.
- (42) Mark, J. E.; Flory, P. J. *J. Am. Chem. Soc.* **1965**, *87*, 1415.
- (43) Helfand, E. *J. Chem. Phys.* **1975**, *62*, 999.
- (44) Matsen, M. W.; Schick, M. *Phys. Rev. Lett.* **1994**, *72*, 2660.
- (45) Semenov, A. N. *Sov. Phys.-JETP (Engl. Transl.)* **1985**, *61*, 733.

MA960105F